

Improved limit on the permanent electric dipole moment of ^{199}Hg

W. C. Griffith,* M. D. Swallows,† T. H. Loftus, M. V. Romalis,‡ B. R. Heckel, and E. N. Fortson§

Department of Physics, University of Washington, Seattle, WA 98195

(Dated: October 23, 2018)

We report the results of a new experimental search for a permanent electric dipole moment of ^{199}Hg utilizing a stack of four vapor cells. We find $d(^{199}\text{Hg}) = (0.49 \pm 1.29_{\text{stat}} \pm 0.76_{\text{sys}}) \times 10^{-29} e \text{ cm}$, and interpret this as a new upper bound, $|d(^{199}\text{Hg})| < 3.1 \times 10^{-29} e \text{ cm}$ (95% C.L.). This result improves our previous ^{199}Hg limit by a factor of 7, and can be used to set new constraints on CP violation in physics beyond the standard model.

PACS numbers: 11.30.Er, 32.10.Dk, 32.80.Xx, 24.80.+y

The existence of a finite permanent electric dipole moment (EDM) of a particle or atom would violate time reversal symmetry (T), and would also imply violation of the combined charge conjugation and parity symmetry (CP) through the CPT theorem [1, 2, 3]. EDMs are suppressed in the standard model of particle physics (SM), lying many orders of magnitude below current experimental sensitivity. However, it is thought that additional sources of CP violation are needed to account for baryogenesis [4, 5], and many theories beyond the SM, such as supersymmetry [6, 7], naturally predict EDMs within experimental reach.

Experimental searches for EDMs have so far yielded null results. The most precise and significant limits have been set on the EDM of the neutron [8], the electron [9], and the ^{199}Hg atom [10], leading to tight constraints on supersymmetric extensions of the SM [7]. Here we report the first result of a new mercury experiment, $|d(^{199}\text{Hg})| < 3.1 \times 10^{-29} e \text{ cm}$ (95% C.L.), which improves our previous limit [10] by a factor of 7 and provides a yet more exacting probe of possible new sources of CP violation.

^{199}Hg has a 1S_0 electronic ground state and nuclear spin $1/2$. An EDM of the ground state atom would point along the nuclear spin axis and arise mainly from CP violation in the nucleus. We measure the nuclear Larmor frequency ν given by $h\nu = |2\mu B \pm 2dE|$, where μ and d are the ^{199}Hg magnetic and electric dipole moments, and B and E are the magnitudes of external magnetic and electric fields aligned parallel (+) or antiparallel (-) with each other. The signature for $d \neq 0$ is thus a shift in Larmor frequency when \vec{E} is reversed relative to \vec{B} .

As shown in Fig. 1, our new apparatus uses a stack of four spin-polarized Hg vapor cells in a common B -field. The middle two cells have oppositely directed E -fields, resulting in EDM-sensitive Larmor shifts of opposite sign; the outer two cells, enclosed by the high voltage (HV) electrodes and thus placed at $E = 0$, are free of EDM effects and serve to cancel B -field gradient noise and provide checks for spurious HV-correlated B -field shifts.

The vapor cells are constructed from high purity fused silica and contain isotopically enriched ^{199}Hg (92 %) at a density of $4 \times 10^{13} \text{ cm}^{-3}$, a paraffin wall coating, and 475 Torr of CO buffer gas. CO efficiently quenches excited

state ^{199}Hg and thus reduces degradation of the wall coating [11]. Spin coherence times T_2 are 100 to 200 sec. A conductive SnO coating on the cell end-caps provides electric field plates separated by 11 mm. The average leakage currents across the cells are 0.42 pA at $\pm 10 \text{ kV}$.

The vapor cells are housed inside a conductive vessel. Upper and lower feedthroughs connect the electrodes containing the outer cells to a HV supply. Holes in the electrodes provide optical access. All materials are free of measurable magnetic impurities. The vessel and electrodes are constructed from electrically conductive, graphite-filled polyethylene. A gold coated, fused-silica plate creates a groundplane between the two middle cells. To minimize leakage currents, the vessel is either periodically or continuously flushed with SF_6 or N_2 .

Light for polarizing the ^{199}Hg spins and detecting their precession is generated with a 254 nm laser system [12] and directed through each cell with the \hat{k} -vector perpendicular to the precession axis along \vec{B} . During the 30 sec pump phase, the light is circularly polarized, tuned to the center of the ^{199}Hg $^1S_0(F = 1/2) \rightarrow ^3P_1(F = 1/2)$ transition, and amplitude modulated at the 16 Hz Larmor frequency set by the 22 mG main magnetic field, thereby

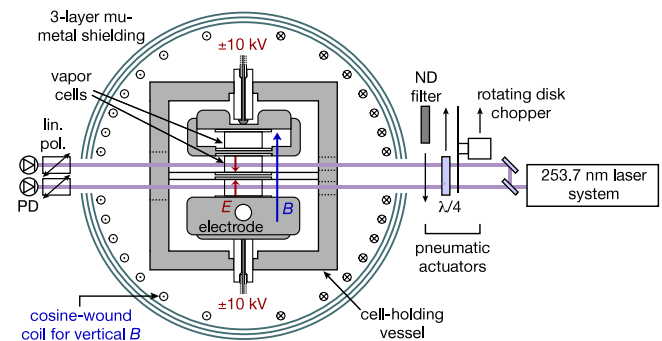


FIG. 1: (Color online) Simplified diagram of the ^{199}Hg EDM apparatus showing details of the vapor cell holding vessel and middle cell light beams. The topmost cell is shown inside a cutaway view of the top electrode, while the bottom electrode shows a light access hole for the enclosed cell. The outer cell light beams are not shown but travel along the magnetic shield axis, perpendicular to the middle cell beams.

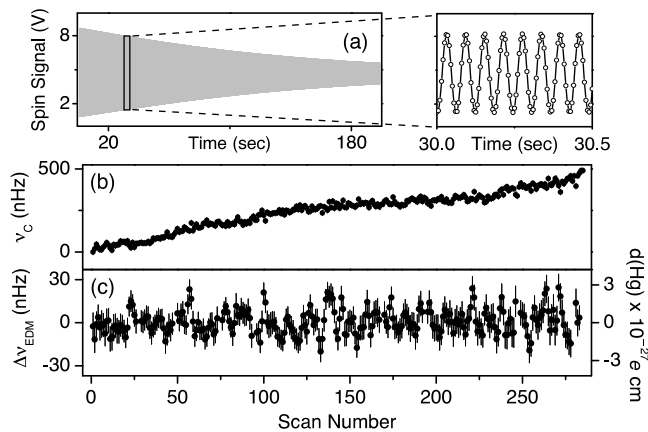


FIG. 2: (a) Typical single-cell precession signal with an expanded 0.5 sec segment. (b) and (c) show ν_c and $\Delta\nu_{EDM}$ for a typical run. In (c) the reduced χ^2 is 1.2 and the run-averaged statistical error is 0.85 nHz after scaling by $\sqrt{\chi^2}$.

building up precession ^{199}Hg spin polarization $\vec{\sigma}$ by synchronous optical pumping. During the probe phase, the light polarization is switched to linear and the frequency is tuned midway between the $F = 1/2$ and $3/2$ hyperfine lines, a detuning that gives large optical rotation angles (proportional to $\vec{\sigma} \cdot \hat{k}$), vanishing circular dichroism, and relatively low absorption. The precession of $\vec{\sigma}$ modulates the light polarization angle at the Larmor frequency; the angle is measured, for each cell, by a photodiode after a linear polarizer. The spin precession is monitored for 100–200 sec, after which the pump/probe cycle is repeated. The HV is ramped to a new value during the pump phase, typically alternating between ± 10 kV.

The Larmor frequencies and their errors are extracted by fitting exponentially decaying sine waves to the photodiode signals. Linear combinations of the fitted frequencies are then constructed. The combination that maximally suppresses magnetic gradient noise, and thus gives the best EDM sensitivity, is $\nu_c = (\nu_{MT} - \nu_{MB}) - \frac{1}{3}(\nu_{OT} - \nu_{OB})$, where the subscripts denote cell positions: *OT* is outer-top, *MB* is middle-bottom, etc. The factor of $\frac{1}{3}$ results from the three times greater separation between the two outer cells compared to the middle cells. Combinations with zero EDM sensitivity are simultaneously used to look for systematic effects. The EDM signal $\Delta\nu_{EDM}$ is obtained from the HV-correlated component of ν_c via 3-point string analysis that removes linear drifts in time [13]. Figure 2 shows a single-cell precession signal for an individual scan, along with ν_c and $\Delta\nu_{EDM}$ for a typical run. Data runs lasted roughly 24 hours and consisted of several hundred individual scans. The run-averaged statistical error for $\Delta\nu_{EDM}$ is set by the weighted error of the mean multiplied by the square root of the reduced χ^2 (for typical runs, χ^2 was 2 or less).

Key components were periodically changed or reversed, with data taken for nine vapor cells, four electrodes, two

vessels, multiple vapor cell and electrode orientations, and various configurations of the photodiode data acquisition (DAQ) channels. The vapor cell, electrode, and vessel flips used nominally identical components. Component changes were made between groups of 10–20 runs termed sequences; in parallel, the paraffin inside each cell was remelted and the outer surfaces of the cells were cleaned. Each sequence comprised a roughly equal number of dipole HV runs (+−+− HV sequence) for the two main *B*-field directions; one or more runs with a quadrupole HV sequence (0+0−0+), sensitive to E^2 effects; and several tilted field (TF) dipole HV runs with the main *B*-field tipped by $\pm 10^\circ$ along the middle and outer light beam \hat{k} -vectors, sensitive to $\vec{v} \times \vec{E}$ motional *B*-fields. A limited number of dipole HV runs were taken at 7 kV and 5 kV. The TF runs and two sequences at high light intensity (used to set limits on intensity-dependent shifts) were excluded from the final value for $\Delta\nu_{EDM}$ due to susceptibility to additional systematic errors.

An unknown, HV-correlated, EDM-mimicking offset was added to the fitted values of ν_{MT} and ν_{MB} . This fixed blind offset masked the measured EDM and was revealed only after the data collection, data cuts, and error analysis were complete.

A potential correlation ($> 90\%$ probability) was found between $\Delta\nu_{EDM}$ and the number of micro-sparks per scan. Nearly every spark, logged as short duration, > 100 pA spikes in the continuously monitored leakage currents, occurred in 5 sequences when the vessel was periodically flushed with N_2 . Two approaches to removing this apparent correlation were tested: one cut individual scans where sparks occurred, the other cut entire sequences containing scans with sparks. The resulting central values for $\Delta\nu_{EDM}$ in the two approaches agreed to

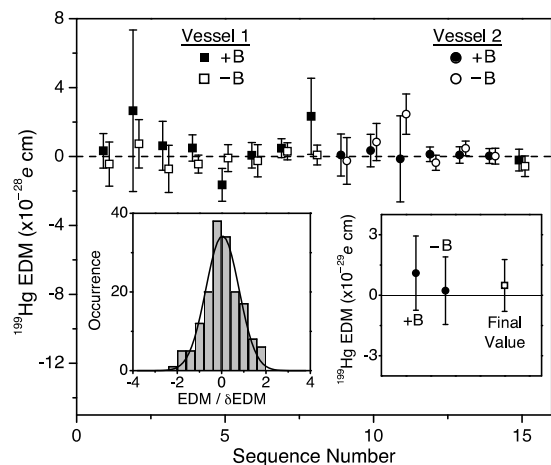


FIG. 3: ^{199}Hg EDM versus sequence number. Open (closed) symbols denote +*B* (−*B*). Squares (circles) denote vessel 1 (vessel 2). The lower-left inset is a histogram of $d(^{199}\text{Hg})$ for the 166 separate runs. The lower-right inset shows the dataset-wide +*B* and −*B* values along with the final $d(^{199}\text{Hg})$.

within 1.8×10^{-30} e cm. The change to $\Delta\nu_{EDM}$ with and without spark cuts was $< 4.2 \times 10^{-30}$ e cm. We adopted the more conservative sequence-elimination approach.

Figure 3 shows $d(^{199}\text{Hg})$ for the 15 sequences that passed the selection criteria, along with a histogram of $d(^{199}\text{Hg})$ for the corresponding 166 runs. The sequence values are divided into one point for each B -field direction; each point is the weighted average of the relevant runs within the sequence. In each case, the $+B$ and $-B$ data are in good agreement. As shown in the lower right inset, the weighted average of all the $+B$ and $-B$ data also agree within $1\text{-}\sigma$. Systematics that change sign (relative to the EDM signal) when B is reversed would appear in the difference, but cancel in the average of the $+B$ and $-B$ results. Although the data is apparently free of such problems, we determined sequence-level values from straight averages of the $+B$ and $-B$ data. The central value for the entire dataset was then obtained from the weighted average of the sequence values: $d(^{199}\text{Hg}) = (0.49 \pm 1.29_{stat}) \times 10^{-29}$ e cm. The statistical error corresponds to a frequency difference between the two middle cells of 0.1 nHz, a $4\times$ improvement on Ref. [10].

With individual run errors set as discussed above, the reduced χ^2 for the 166 runs is 0.65. When the individual scans are grouped into 3 hour segments and the same procedure is applied, $\chi^2 \sim 1$. One potential source of this behavior is low frequency drift that averages faster than white noise, due for example to beam pointing drift that is tied to the 3 hour time scale for resets of the piezo-actuated laser cavity mirrors.

Figure 4 summarizes several checks for systematic effects. We did not find statistically significant correlations between $\Delta\nu_{EDM}$ and the vapor cells or electrodes (or their orientation inside the vessel), the DAQ channel ordering, or the vessels. Values for $d(^{199}\text{Hg})$ extracted from the TF runs, the quadrupole HV runs, the high intensity runs, and the two-cell difference, MD = $(\nu_{MT} - \nu_{MB})$, agree with the Fig. 3 final value at the $1\text{-}\sigma$ level.

Table I summarizes the systematic errors. Three contributions dominate. The *spark analysis* error is the difference in the final $\Delta\nu_{EDM}$ value with and without spark cuts. The *parameter correlations* error is obtained by multiplying the HV correlation for key experimental parameters by the correlation of each parameter with $\Delta\nu_{EDM}$, and then summing the products in quadrature. Specific parameters are: the vapor cell spin amplitudes, lifetimes, relative phases, and light transmission; the laser power, frequency, drive current, and piezo control voltages; an external 3-axis fluxgate magnetometer; and the B -field coil currents (main coil and 3 gradient coils). No statistically significant correlations were found. The *leakage current* induced error cannot be obtained from the (unresolved) correlation slope of $\Delta\nu_{EDM}$ versus leakage current due to the limited range over which the currents varied. A conservative estimate is instead obtained from the worst case scenario of current flow along heli-

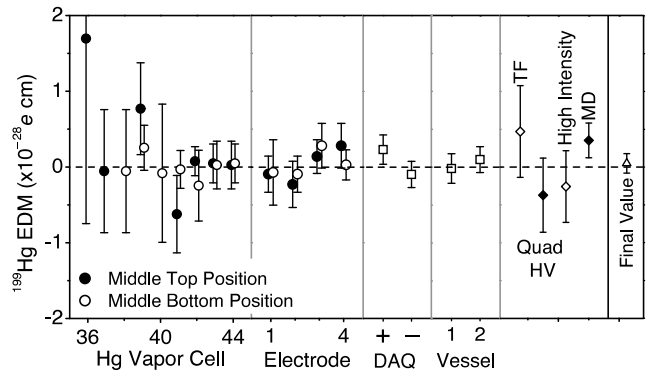


FIG. 4: Dependence of $d(^{199}\text{Hg})$ on the vapor cells, electrodes, DAQ channel order, and vessels. The second pane from the right shows $d(^{199}\text{Hg})$ extracted from the quadrupole HV, high intensity, and TF runs and the two-cell difference (MD). The right-most pane shows the final $d(^{199}\text{Hg})$ described in the text.

cal paths within or on the vapor cell walls. The vapor cell geometry, with two opposed seal-off stems, limits a helical current path to $\leq 1/2$ full turn around the cell. The average single-cell leakage current was 0.42 pA. The resulting fields in the two middle cells can either add or subtract, so we take $\sqrt{2} \times 0.42$ pA = 0.59 pA as the effective current. The measurement used 9 different vapor cells (4 dominate the statistical error) whose helical current paths should be uncorrelated; to account for this averaging, we divide by 2. Combining the above gives a systematic error of 4.53×10^{-30} e cm. The remaining Table I entries will be discussed in a longer publication.

Summing the systematic errors in quadrature leads to our final result:

$$d(^{199}\text{Hg}) = (0.49 \pm 1.29_{stat} \pm 0.76_{syst}) \times 10^{-29} \text{ e cm},$$

which we interpret as an upper limit of $|d(^{199}\text{Hg})| < 3.1 \times 10^{-29}$ e cm (95% C.L.). This new limit can be translated into upper bounds on more fundamental CP violating parameters. Table II summarizes these limits.

CP violation in atomic nuclei is conventionally parameterized by the Schiff moment S , the lowest order CP violating nuclear moment unscreened by the electron cloud. Atomic calculations give $d(^{199}\text{Hg}) = -2.8 \times 10^{-17}(S/e\text{fm}^3)$ e cm [23]. The dominant contribution to the ^{199}Hg Schiff moment is expected to come

TABLE I: Systematic error budget (10^{-30} e cm).

Source	Error	Source	Error
Leakage Currents	4.53	Charging Currents	0.40
Parameter Correlations	4.31	Convection	0.36
Spark Analysis	4.16	$(\vec{v} \times \vec{E})$ B -Fields	0.18
Stark Interference	1.09	Berry's Phase	0.18
E^2 Effects	0.62	Quadrature Sum	7.63

TABLE II: Limits on CP violating parameters based on our new experimental limit for $d(^{199}\text{Hg})$ (95% C.L.) compared to limits from the Tl (90% C.L.) [9], neutron (90% C.L.) [8], or TlF (95% C.L.) [14] experiments. Values that improve upon (complement) previous limits appear above (below) the horizontal line. Relevant theory references for the alternate limits are given in the last column.

Parameter	^{199}Hg bound	Hg theory	Best alternate limit
$\tilde{d}_q(\text{cm})$ ^a	6×10^{-27}	[15]	n: 3×10^{-26} [3]
$d_p(e \text{ cm})$	7.9×10^{-25}	[16]	TlF: 6×10^{-23} [17]
C_S	5.2×10^{-8}	[18]	Tl: 2.4×10^{-7} [19]
C_P	5.1×10^{-7}	[18]	TlF: 3×10^{-4} [1]
C_T	1.5×10^{-9}	[18]	TlF: 4.5×10^{-7} [1]
$\bar{\theta}_{QCD}$	3×10^{-10}	[20]	n: 1×10^{-10} [3]
$d_n(e \text{ cm})$	5.8×10^{-26}	[16]	n: 2.9×10^{-26} [3]
$d_e(e \text{ cm})$	3×10^{-27}	[21, 22]	Tl: 1.6×10^{-27} [18]

^aFor ^{199}Hg : $\tilde{d}_q = (\tilde{d}_u - \tilde{d}_d)$, while for n: $\tilde{d}_q = (0.5\tilde{d}_u + \tilde{d}_d)$.

from CP violating nucleon-nucleon interactions. The most recent calculation gives $S(^{199}\text{Hg}) = g(0.01\bar{g}^{(0)} + 0.07\bar{g}^{(1)} + 0.02\bar{g}^{(2)})e\text{fm}^3$ [24], where g is the strong pion-nucleon-nucleon (πNN) coupling constant, and \bar{g} denotes CP -odd πNN isoscalar (0), isovector (1), and isotensor (2) couplings. Note that recent work considers whether the form of S used to interpret atomic EDMs should be modified [25, 26]. The isovector coupling has been calculated in terms of chromo-EDMs of the quarks, giving $\bar{g}^{(1)} = 2(\tilde{d}_u - \tilde{d}_d)10^{14} \text{ cm}^{-1}$ [15]. For comparison, the neutron EDM is dependent on a different combination of quark EDMs and chromo-EDMs, $d_n = 1.1e(0.5\tilde{d}_u + \tilde{d}_d) + 1.4(d_d - 0.25d_u)$ [3]. The quark EDMs and chromo-EDMs can be estimated in supersymmetric extensions of the SM and in many cases, our result for $d(^{199}\text{Hg})$ provides the most stringent constraints on CP violating phases [3, 6, 7]. The isoscalar coupling is dependent on the CP violating phase in the QCD Lagrangian, $\bar{g}^{(0)} \simeq 0.027\bar{\theta}_{QCD}$ [20].

Although expected to be smaller than the above effects, the proton and neutron EDM contributions to S were calculated in [16] giving $S(^{199}\text{Hg}) = (1.9d_n + 0.2d_p) \text{ fm}^2$. This allows us to set limits, $|d_n| < 5.8 \times 10^{-26} e \text{ cm}$ and $|d_p| < 7.9 \times 10^{-25} e \text{ cm}$, where in the case of the proton we include a 30% theoretical uncertainty as in [16]. This improves the best upper limit on d_p by a factor of 7.

The ^{199}Hg EDM can also have possible contributions from CP violating semileptonic interactions between the atomic electrons and nucleons, typically parameterized in terms of the constants C_S , C_P , and C_T [1, 18]. New bounds on these parameters are shown in Table II. We also present a limit on the electron EDM derived from the hyperfine structure coupling between the nuclear and electronic spins, $d(^{199}\text{Hg}) \simeq 0.012d_e$ [22]. This limit, however, is relatively uncertain since an alternate estimate is of opposite sign, $d(^{199}\text{Hg}) \simeq -0.014d_e$ [1, 21].

In summary, we have performed a new search for the ^{199}Hg EDM. We improve the previous limit by a factor of 7, placing new bounds on hadronic and semileptonic CP violation. We are currently upgrading the apparatus and expect further improvements in the EDM sensitivity.

This work was supported by NSF Grant PHY-0457320 and the DOE Office of Nuclear Science. We gratefully acknowledge contributions by Laura Kogler, Eric Lindahl, David Meyer, Bob Morley, and Kristian Wædegaard.

* Present address: NIST, Boulder, CO 80305

† Present address: JILA, Univ. of CO, Boulder, CO 80309

‡ Permanent address: Department of Physics, Princeton University, Princeton, NJ 08544

§ Email: fortson@phys.washington.edu

- [1] I. P. Khriplovich and S. K. Lamoreaux, *CP Violation Without Strangeness* (Springer, Berlin, 1997).
- [2] P. G. H. Sandars, *Contemp. Phys.* **42**, 97 (2001).
- [3] M. Pospelov and A. Ritz, *Ann. Phys. (N.Y.)* **318**, 119 (2005).
- [4] M. Trodden, *Rev. Mod. Phys.* **71**, 1463 (1999).
- [5] S. J. Huber, M. Pospelov, and A. Ritz, *Phys. Rev. D* **75**, 036006 (2007).
- [6] S. M. Barr, *Int. J. Mod. Phys. A* **8**, 209 (1993).
- [7] K. A. Olive, M. Pospelov, A. Ritz, and Y. Santoso, *Phys. Rev. D* **72**, 075001 (2005).
- [8] C. A. Baker *et al.*, *Phys. Rev. Lett.* **97**, 131801 (2006).
- [9] B. C. Regan, E. D. Commins, C. J. Schmidt, and D. DeMille, *Phys. Rev. Lett.* **88**, 071805 (2002).
- [10] M. V. Romalis, W. C. Griffith, J. P. Jacobs, and E. N. Fortson, *Phys. Rev. Lett.* **86**, 2505 (2001).
- [11] M. V. Romalis and L. Lin, *J. Chem. Phys.* **120**, 1511 (2004).
- [12] D. M. Harber and M. V. Romalis, *Phys. Rev. A* **63**, 013402 (2000).
- [13] M. Swallows, Ph.D. thesis, Univ. of Washington (2007).
- [14] D. Cho, K. Sangster, and E. A. Hinds, *Phys. Rev. A* **44**, 2783 (1991).
- [15] M. Pospelov, *Phys. Lett. B* **530**, 123 (2002).
- [16] V. F. Dmitriev and R. A. Sen'kov, *Phys. Rev. Lett.* **91**, 212303 (2003).
- [17] A. N. Petrov *et al.*, *Phys. Rev. Lett.* **88**, 073001 (2002).
- [18] J. S. M. Ginges and V. V. Flambaum, *Phys. Rep.* **397**, 63 (2004).
- [19] B. K. Sahoo *et al.*, *Phys. Rev. A* **78**, 010501 (2008); **78**, 039901(E) (2008).
- [20] R. J. Crewther, P. Di Vecchia, and G. Veneziano, *Phys. Lett. B* **88**, 123 (1979); **91**, 487(E) (1980).
- [21] V. V. Flambaum and I. B. Khriplovich, *Sov. Phys. JETP* **62**, 872 (1985).
- [22] A.-M. Martensson-Pendrill and P. Öster, *Phys. Scr.* **36**, 444 (1987).
- [23] V. A. Dzuba, V. V. Flambaum, J. S. M. Ginges, and M. G. Kozlov, *Phys. Rev. A* **66**, 012111 (2002).
- [24] J. H. de Jesus and J. Engel, *Phys. Rev. C* **72**, 045503 (2005).
- [25] C.-P. Liu *et al.*, *Phys. Rev. C* **76**, 035503 (2007).
- [26] R. A. Sen'kov, N. Auerbach, V. V. Flambaum, and V. G. Zelevinsky, *Phys. Rev. A* **77**, 014101 (2008).